PHILOSOPHICAL TRANSACTIONS A

Modelling of stiffness degradation due to cracking in laminates subjected to multi-axial loading

Journal:	*Philosophical Transactions A*
Manuscript ID	Draft
Article Type:	Research
Date Submitted by the Author:	n/a
Complete List of Authors:	Kashtalyan, Maria; University of Aberdeen, School of Engineering Soutis, Constantinos; University of Manchester, Aerospace Research Institute
Issue Code: Click here to find the code for your issue.:	TM0116
Subject:	Mechanical engineering < ENGINEERING AND TECHNOLOGY, Materials science < ENGINEERING AND TECHNOLOGY
Keywords:	Polymer-matrix composites, fibre-reinforced composites, composite laminates, matrix cracking, delamination

SCHOLARONE™
Manuscripts

PHILOSOPHICAL TRANSACTIONS A

Phil. Trans. R. Soc. A.
doi:10.1098/not yet assigned

Modelling of stiffness degradation due to cracking in laminates subjected to multi-axial loading

M. Kashtalyan[1], C. Soutis[2]

[1]*Centre for Micro- and Nanomechanics (CEMINACS), School of Engineering, University of Aberdeen, UK*
[2]*Aerospace Research Institute, The University of Manchester, Manchester, UK*

Keywords: Polymer-matrix composites; fibre-reinforced composites; composite laminates; matrix cracking; delamination

The paper presents an analytical approach to predicting the effect of intra- and interlaminar cracking on residual stiffness properties of the laminate, which can be used in the post-initial failure analysis, taking full account of damage mode interaction. The approach is based on a two-dimensional shear lag stress analysis and the Equivalent Constraint Model of the laminate with multiple damaged plies. The application of the approach to predicting degraded stiffness properties of multidirectional laminates under multi-axial loading is demonstrated on cross-ply glass/epoxy and carbon/epoxy laminates with transverse and longitudinal matrix cracks and crack-induced transverse and longitudinal delaminations.

Introduction

Failure process of fibre-reinforced composite laminates subjected to multi-axial loading involves sequential accumulation of intra- and interlaminar damage in the form of matrix cracking and delamination. Intralaminar matrix cracks parallel to the fibres in the off-axis plies is the first damage mode observed. Depending on the laminate stacking sequence, these cracks are either arrested at the interface or cause interfacial failure leading to delamination and/or cracking in the adjacent layers due to high interlaminar stresses at the interface.

Development of intra- and interlaminar damage in composite laminates has been the subject of numerous studies in the literature, see e.g. our reviews [1, 2]. More recently, Rebiere and Gamby [3, 4] proposed an energy criterion based on the computation of the partial strain energy release rates associated with transverse cracking, longitudinal cracking and crack-induced delamination and used it to predict initiation of these damage modes in symmetric cross-ply laminates subjected to uniaxial loading. Lim and Li [5] evaluated the energy release rate associated with matrix cracking and crack-induced delamination and used them to critically evaluate damage mode transition from transverse cracking to delamination. Blazques et al [6] employed boundary element method to carry out a numerical study of the stress state in the neighbourhood of matrix crack-induced delamination in a cross-ply laminate in order to clarify the mechanisms of damage interaction between transverse cracking and delamination. Maimi et al [7, 8] carried out a comprehensive study of matrix cracking and crack-induced delaminatons, proposing a model to simulate stress-strain state of the damaged ply and using it to analyse evolution of matrix cracking and crack-induced delamination. Garcia et al [9] modelled transverse cracking onset and growth in cross-ply laminates using a coupled stress and energy criterion. Intra- and interlaminar cracking in composite laminates under impact loading and four point bending was investigated by Shi et al [10] and Shi and Soutis [11], respectively.

Multidirectional laminates subjected to multiaxial loading may still be capable of carrying load after matrix cracking has occurred. In the laminate, in-plane shear and normal stresses can be transferred, to some extent, back into the damaged lamina via the neighbouring laminae. Owing to this stress transfer damaged lamina within the laminate retains certain amount of load-carrying capacity. In-situ stiffness of a damaged lamina constrained within the laminate depends on the damage configuration and stiffnesses and thicknesses of neighbouring laminae. Prediction of the post-initial failure behaviour of a laminate requires accurate information regarding the properties of the damaged lamina.

This paper describes a method of predicting the effect of intra- and inter-laminar damage on the stiffness properties of the laminate which can be used in the post-initial failure analysis, taking full account of damage mode interaction. The approach is based on the Equivalent Constraint Model (ECM) of the damaged laminate [12-21]. Closed form expressions

*Author for correspondence (m.kashtalyan@abdn.ac.uk).

are given for the In-situ Damage Effective Functions which characterise degraded stiffness properties of each damaged ply; for a given damaged ply they explicitly depend on the damage parameters (matrix crack density and relative delamination area) associated with that ply and implicitly on the damage parameters associated with other damaged plies.

The application of the approach to predict the degraded stiffness properties of multidirectional laminate with multilayer inter- and interlaminar damage is shown for cross-ply glass/epoxy and carbon/epoxy laminates damaged by transverse and longitudinal matrix cracks and crack-induced transverse and longitudinal delamination.

Equivalent Constraint Model

Figure 1 shows a schematic of the cross-ply $[0_m/90_n]_s$ laminate damaged by transverse and longitudinal delaminations growing from the tips of transverse cracks in the 90° plies and longitudinal cracks in the 0° plies. Transverse and longitudinal cracks are assumed to be spaced uniformly and to span the full thickness and width of the 90° and 0° plies, while delaminations are assumed strip-shaped. Spacings between longitudinal and transverse cracks are denoted respectively $2s_1$ and $2s_2$, while the length of longitudinal and transverse delaminations are denoted $2\ell_1$ and $2\ell_2$, respectively. A set of Cartesian co-ordinates with the origin in the centre of the laminate is introduced, with x_1-axis coinciding with the fibre direction in the 90° lamina and x_3-axis directed through the laminate thickness. The laminate is subjected to general in-plane biaxial tension ($\overline{\sigma}_{11}$ and $\overline{\sigma}_{22}$) and shear loading ($\overline{\sigma}_{12}$).

In order to analyse in-situ constrain effect on the stiffness of a particular cracked lamina, the Equivalent Constraint Model (ECM) of the damaged laminate is employed [22-24]. In the ECM laminate, all the laminae below and above the damaged lamina under consideration are replaced with homogeneous layers (I and II) having the equivalent constraining effect (Fig. 2). In-plane stiffness properties of the equivalent constraint layer can be obtained from the laminated plate theory once their stresses and strains are known from micromechanical analysis. Theoretically, ECM does not impose any restrictions onto the laminate lay-up, and the approach was applied to analysis of quasi-isotropic laminate with matrix cracking in all but $0°$ layers by Zhang and Herrmann [25].

Application of the ECM approach to cross-ply laminate damaged by transverse and longitudinal matrix cracks and transverse and longitudinal crack-induced delaminations is schematically shown in Fig. 3. Instead of considering the damaged laminate configuration shown on Fig. 1, the following two ECMs are analysed instead. In ECM1 (Fig. 3a), the 0° lamina (layer 1) contains damage explicitly, while 90° lamina (layer 2), damaged by transverse cracking and transverse delaminations, is replaced with the homogeneous layer with reduced stiffness properties. Likewise, in ECM2 (Fig. 3b), the 90° lamina (layer 2) is damaged explicitly, while the damaged 0° lamina is replaced with the homogeneous layer with reduced stiffness. All the quantities associated with the 0° lamina (layer 1) will be henceforth denoted by a sub- or superscript (1), whereas those associated with the 90° lamina (layer 2) with a sub- or superscript (2).

The reduced stiffness properties of the μ^{th} layer ($\mu = 1, 2$) damaged by transverse cracking and transverse delaminations (if $\mu = 2$) or splitting and longitudinal delamination (if $\mu = 1$) can be calculated from the laminated plate theory, provided stresses and strains in the explicitly damaged μ^{th} layer are known from the analysis of the $\text{ECM}\mu$ (i.e. ECM1 if $\mu = 1$ and ECM2 if $\mu = 2$). The reduced elastic properties of the equivalently constraining layer $\kappa, \kappa \neq \mu$ required in the analysis of the $\text{ECM}\mu$ are supposed to be determined from the analysis of the $\text{ECM}\kappa$. Thus, the problems for ECM1 and ECM2 are inter-related, damage coupling effect is included in the residual stiffness analysis.

Stress analysis

Due to the periodicity of damage configuration in the $\text{ECM}\mu$, only their representative segments (Fig. 3), containing either a pair of splits or a single transverse crack as well as two strip-shaped delaminations, need to be considered. As the representative segments are symmetric with respect to the mid-plane and their material and geometry are noteworthy uniform in direction perpendicular to the $x_\mu 0 x_3$ plane, the analysis can be further restricted to one quarter of the representative segments. The representative segments of ECM1 and ECM2 can be segregated into perfectly bonded ($\ell_\mu < |x_\mu| < s_\mu$) regions and locally delaminated ($|x_\mu| < \ell_\mu$, $\mu = 1,2$) regions, with no frictional contact between the layers in the latter.

In the perfectly bonded regions ($\ell_\mu < |x_\mu| < s_\mu$) of the $\text{ECM}\mu$, stresses can be determined from the equilibrium equations

$$\frac{d}{dx_\mu}\tilde{\sigma}_{j\mu}^{(\mu,k)} + (-1)^k \frac{\tau_j^{(\mu)}}{h_k} = 0, \quad \mu = 1,2 \quad j = 1,2 \quad k = 1,2 \tag{1}$$

Here $\tau_j^{(\mu)}$ are the peak shear stresses at the (0/90) interface of the $\mathrm{ECM}\mu$ in the $x_\mu 0 x_3$ plane; $\tilde{\sigma}_{pq}^{(\mu,k)}$, $p,q = 1,2$ are the in-plane microstresses in the k^{th} layer of the $\mathrm{ECM}\mu$, i.e. the stresses averaged across the thickness of the k^{th} layer and the width of the $\mathrm{ECM}\mu$ as indicated below

$$\tilde{\sigma}_{pq}^{(\mu,k)} = \frac{1}{2w_\mu h_k}\int_{h_k}\int_{w_\mu} \sigma_{pq}^{(\mu,k)} dx_3 dx_k, \quad p,q = 1,2 \tag{2}$$

In the locally delaminated region ($|x_\mu| \le \ell_\mu$) of the $\mathrm{ECM}\mu$, the in-plane microstresses in the explicitly damaged μ^{th} layer vanish, i.e.

$$\tilde{\sigma}_{j\mu}^{(\mu,\mu)} = 0, \quad j,\mu = 1,2 \tag{3}$$

The in-plane microstresses are related to the total stresses $\bar{\sigma}_{ij}$ applied to the laminate by the following equilibrium equations

$$\chi\tilde{\sigma}_{ij}^{(\mu,1)} + \tilde{\sigma}_{ij}^{(\mu,2)} = (1+\chi)\bar{\sigma}_{ij}, \quad i,j = 1,2 \quad \chi = h_1/h_2 \tag{4}$$

It is assumed that both the explicitly damaged and the equivalently constraining laminae in the $\mathrm{ECM}\mu$ are homogeneous orthotropic, and their constitutive equations, in terms of the in-plane microstresses and microstrains, can be written as

$$\begin{Bmatrix} \tilde{\sigma}_1^{(\mu,\mu)} \\ \tilde{\sigma}_2^{(\mu,\mu)} \\ \tilde{\sigma}_6^{(\mu,\mu)} \end{Bmatrix} = \begin{bmatrix} \hat{Q}_{11}^{(\mu)} & \hat{Q}_{12}^{(\mu)} & 0 \\ \hat{Q}_{12}^{(\mu)} & \hat{Q}_{22}^{(\mu)} & 0 \\ 0 & 0 & \hat{Q}_{66}^{(\mu)} \end{bmatrix} \begin{Bmatrix} \tilde{\varepsilon}_1^{(\mu,\mu)} \\ \tilde{\varepsilon}_2^{(\mu,\mu)} \\ \tilde{\varepsilon}_6^{(\mu,\mu)} \end{Bmatrix} \tag{5a}$$

$$\begin{Bmatrix} \tilde{\sigma}_1^{(\mu,\kappa)} \\ \tilde{\sigma}_2^{(\mu,\kappa)} \\ \tilde{\sigma}_6^{(\mu,\kappa)} \end{Bmatrix} = \begin{bmatrix} Q_{11}^{(\kappa)} & Q_{12}^{(\kappa)} & 0 \\ Q_{12}^{(\kappa)} & Q_{22}^{(\kappa)} & 0 \\ 0 & 0 & Q_{66}^{(\kappa)} \end{bmatrix} \begin{Bmatrix} \tilde{\varepsilon}_1^{(\mu,\kappa)} \\ \tilde{\varepsilon}_2^{(\mu,\kappa)} \\ \tilde{\varepsilon}_6^{(\mu,\kappa)} \end{Bmatrix} \quad \mu,\kappa = 1,2, \quad \kappa \ne \mu \tag{5b}$$

where $[\hat{Q}^{(\mu)}]$ denotes the in-plane stiffness matrix of the explicitly damaged μ^{th} layer (a circumflex (^) is used for representing the elastic properties of the undamaged material), and $[Q^{(\kappa)}], \kappa \ne \mu$ denotes the in-plane stiffness matrix of the homogeneous orthotropic material of the equivalently constraining κ^{th} layer. The in-plane constitutive equations can also be written in terms of strains as

$$\begin{Bmatrix} \tilde{\varepsilon}_1^{(\mu,\mu)} \\ \tilde{\varepsilon}_2^{(\mu,\mu)} \\ \tilde{\varepsilon}_6^{(\mu,\mu)} \end{Bmatrix} = \begin{bmatrix} \hat{S}_{11}^{(\mu)} & \hat{S}_{12}^{(\mu)} & 0 \\ \hat{S}_{12}^{(\mu)} & \hat{S}_{22}^{(\mu)} & 0 \\ 0 & 0 & \hat{S}_{66}^{(\mu)} \end{bmatrix} \begin{Bmatrix} \tilde{\sigma}_1^{(\mu,\mu)} \\ \tilde{\sigma}_2^{(\mu,\mu)} \\ \tilde{\sigma}_6^{(\mu,\mu)} \end{Bmatrix} \tag{6a}$$

$$\begin{Bmatrix} \tilde{\varepsilon}_1^{(\mu,\kappa)} \\ \tilde{\varepsilon}_2^{(\mu,\kappa)} \\ \tilde{\varepsilon}_6^{(\mu,\kappa)} \end{Bmatrix} = \begin{bmatrix} S_{11}^{(\kappa)} & S_{12}^{(\kappa)} & 0 \\ S_{12}^{(\kappa)} & S_{22}^{(\kappa)} & 0 \\ 0 & 0 & S_{66}^{(\kappa)} \end{bmatrix} \begin{Bmatrix} \tilde{\sigma}_1^{(\mu,\kappa)} \\ \tilde{\sigma}_2^{(\mu,\kappa)} \\ \tilde{\sigma}_6^{(\mu,\kappa)} \end{Bmatrix} \quad \kappa,\mu = 1,2 \quad \kappa \ne \mu \tag{6b}$$

where $[\hat{S}^{(\mu)}]$, $[S^{(\kappa)}], \kappa \ne \mu$ denote the in-plane compliance matrices of the explicitly damaged μ^{th} layer and equivalently constraining κ^{th} layer, respectively.

In order to determine the in-plane microstresses in the perfectly bonded region from the equilibrium equations, Eq. (1), the interface shear stresses $\tau_j^{(\mu)}$ are expressed in terms of in-plane displacements $u_j^{(\mu,k)}$, $j = 1,2$. Here, it is assumed that

the out-of-plane shear stresses $\sigma_{j3}^{(\mu,k)}$, $j=1,2$ vary linearly with x_3, which corresponds to a parabolic variation of the in-plane displacements. Besides that, it is assumed that in the 0^o-lamina linear variation of the out-of-plane shear stresses $\sigma_{j3}^{(\mu,1)}$, $j=1,2$, is restricted to the region of about one ply thickness (i.e. the nominal thickness of the pre-preg used to make the laminate). We assume that all layers of the laminate have thicknesses in the multiples of the nominal ply thickness. For laminates with thick 0^o-layer this appears to offer a more reasonable description of the cracked laminate behaviour. Thus, here the out-of-plane shear stresses are assumed to vary as follows

$$\sigma_{j3}^{(\mu,2)}=\frac{\tau_j^{(\mu)}}{h_2}x_3 \quad |x_3|\le h_2 \quad \sigma_{j3}^{(\mu,1)}=\frac{\tau_j^{(\mu)}}{h_s}(h_2+h_s-x_3) \quad h_2\le|x_3|\le h_2+h_s$$
$$\sigma_{j3}^{(\mu,1)}=0 \quad h_2+h_s\le|x_3|\le h_2+h_1 \qquad h_s=m_s t \qquad j=1,2 \tag{7}$$

where h_s is the thickness of the shear layer, m_s is the number of plies in the shear layer, and t is the ply thickness. After some mathematical calculations and equation rearrangements (see, e.g., Appendix A in [26]), the interface shear stresses are obtained as

$$\tau_j^{(\mu)}=K_j^{(\mu)}(\tilde{u}_j^{(\mu,1)}-\tilde{u}_j^{(\mu,2)}) \tag{8}$$

where the shear lag parameters K_j are functions of ply properties

$$K_j=\frac{3\hat{G}_{j3}^{(1)}\hat{G}_{j3}^{(2)}}{h_2\hat{G}_{j3}^{(1)}+(1+(1-\eta)/2)\eta h_1\hat{G}_{j3}^{(2)}}, \quad \eta=h_s/h_1, \qquad j=1,2 \tag{9}$$

Here, $\hat{G}_{j3}^{(k)}$, $k=1,2$ are the out-of-plane shear moduli of the k^{th} layer. As the presence of aligned microcracks does not affect the value of the out-of-plane shear moduli (this fact is emphasised by marking them with a circumflex (^)), the shear lag parameters K_j are the same for ECM1 and ECM2.

The equilibrium equations, Eq. (1), along with expressions for the interface shear stresses, Eq. (8), the laminate equilibrium equations, Eq. (4), and constitutive equations, Eq. (6), provide a full set of equations, which are required for determining the in-plane microstresses $\tilde{\sigma}_{j\mu}^{(\mu,\mu)}$ $j,\mu=1,2$ in the perfectly bonded regions of the representative segment of the ECMμ. For instance, $\tilde{\sigma}_{11}^{(1,1)}$ can be found from the following set of 8 equations with respect to 8 variables

$$\frac{d\tilde{\sigma}_{11}^{(1,1)}}{dx_1}-\frac{\tau_1^{(1)}}{h_1}=0, \quad \tau_1^{(1)}=K_1(\tilde{u}_1^{(1,1)}-\tilde{u}_1^{(1,2)}) \tag{10a,b}$$

$$\chi\tilde{\sigma}_{11}^{(1,1)}+\tilde{\sigma}_{11}^{(1,2)}=(1+\chi)\bar{\sigma}_{11}, \quad \chi\tilde{\sigma}_{22}^{(1,1)}+\tilde{\sigma}_{22}^{(1,2)}=(1+\chi)\bar{\sigma}_{22} \tag{10c,d}$$

$$\begin{Bmatrix}\dfrac{d\tilde{u}_1^{(1,1)}}{dx_1}\\ \bar{\varepsilon}_2^{(1)}\end{Bmatrix}=\begin{bmatrix}\hat{S}_{11}^{(1)} & \hat{S}_{12}^{(1)}\\ \hat{S}_{12}^{(1)} & \hat{S}_{22}^{(1)}\end{bmatrix}\begin{Bmatrix}\tilde{\sigma}_{11}^{(1,1)}\\ \tilde{\sigma}_{22}^{(1,1)}\end{Bmatrix}, \qquad \begin{Bmatrix}\dfrac{d\tilde{u}_1^{(1,2)}}{dx_1}\\ \bar{\varepsilon}_2^{(1)}\end{Bmatrix}=\begin{bmatrix}S_{11}^{(2)} & S_{12}^{(2)}\\ S_{12}^{(2)} & S_{22}^{(2)}\end{bmatrix}\begin{Bmatrix}\tilde{\sigma}_{11}^{(1,2)}\\ \tilde{\sigma}_{22}^{(1,2)}\end{Bmatrix} \tag{10e,f}$$

After some rearrangement, this and other similar sets of equations can be reduced to the single differential equations

$$\frac{d^2\tilde{\sigma}_{\mu\mu}^{(\mu,\mu)}}{dx_\mu}-L_1^{(\mu)}\tilde{\sigma}_\mu^{(\mu,\mu)}+\Omega_{11}^{(\mu)}\bar{\sigma}_{11}+\Omega_{22}^{(\mu)}\bar{\sigma}_{22}=0, \quad \mu=1,2 \tag{11a}$$

$$\frac{d^2\tilde{\sigma}_{12}^{(\mu,\mu)}}{dx_\mu}-L_2^{(\mu)}\tilde{\sigma}_{12}^{(\mu,\mu)}+\Omega_{12}^{(\mu)}\bar{\sigma}_{12}=0 \tag{11b}$$

where $L_1^{(\mu)}, L_1^{(\mu)}, \Omega_{11}^{(\mu)}, \Omega_{22}^{(\mu)}, \Omega_{12}^{(\mu)}$ are the laminate constants depending on the layer compliances $\hat{S}_{ij}^{(\mu)}, S_{ij}^{(\kappa)}, \kappa \neq \mu$, shear lag parameters K_j and the layer thickness ratio $\chi = h_1 / h_2$. In detail, they are presented in Appendix B of [26]. Given the stress-free boundary conditions at the crack/split surfaces, solutions to Eqs. (11) are

$$\tilde{\sigma}_{\mu\mu}^{(\mu,\mu)} = \frac{1}{L_1^{(\mu)}}\left(1 - \frac{\cosh[\sqrt{L_1^{(\mu)}}(x_\mu - s_\mu)]}{\cosh[\sqrt{L_1^{(\mu)}}(s_\mu - \ell_\mu)]}\right)(\Omega_{11}^{(\mu)}\overline{\sigma}_{11} + \Omega_{22}^{(\mu)}\overline{\sigma}_{22}) \tag{12a}$$

$$\tilde{\sigma}_{12}^{(\mu,\mu)} = \frac{1}{L_2^{(\mu)}}\left(1 - \frac{\cosh[\sqrt{L_2^{(\mu)}}(x_\mu - s_\mu)]}{\cosh[\sqrt{L_2^{(\mu)}}(s_\mu - \ell_\mu)]}\right)\Omega_{12}^{(\mu)}\overline{\sigma}_{12} \tag{12b}$$

where s_μ is crack/split half-spacing and ℓ_μ is crack/split tip delamination half-length (Figs. 1, 3). Once the in-plane microstresses, Eq. (12), in the explicitly damaged μ^{th} layer of the $\text{ECM}\mu$ are known, the laminate macrostresses can be found as

$$\overline{\sigma}_{j\mu}^{(\mu,\mu)} = \frac{1}{2s_\mu}\int_{-s_\mu}^{s_\mu} \tilde{\sigma}_{j\mu}^{(\mu,\mu)} dx_\mu \tag{13}$$

The reduced stiffness properties of the layer μ, damaged by transverse cracking or splitting and delaminations, can be determined by applying the laminate plate theory to the $\text{ECM}\mu$ after replacing the explicitly damaged layer with an equivalent homogeneous one. The constitutive equations for the homogeneous layer equivalent to the explicitly damaged μ^{th} layer are

$$\{\overline{\sigma}^{(\mu,\mu)}\} = [Q^{(\mu)}]\{\overline{\varepsilon}^{(\mu,\mu)}\} \tag{14}$$

Where in order to satisfy compatability the macrostrains are assumed to be

$$\overline{\varepsilon}_j^{(\mu,\mu)} = \overline{\varepsilon}_j^{(\mu,\kappa)} = \overline{\varepsilon}_j = \frac{1}{2s_\mu}\int_{-s_\mu}^{s_\mu} \tilde{\varepsilon}_j^{(\mu,\kappa)} dx_\mu, \quad \kappa \neq \mu, \quad j = 1,2,6 \tag{15}$$

Stiffness of a damaged lamina

The in-plane reduced stiffness matrix $[Q^{(\mu)}]$ of the homogeneous layer equivalent to the μ^{th} layer of the $\text{ECM}\mu$ is

$$[Q^{(\mu)}] = [\hat{Q}^{(\mu)}] - [R^{(\mu)}] \tag{16}$$

$$[R^{(1)}] = \begin{bmatrix} \hat{Q}_{11}^{(1)}\Lambda_{22}^{(1)} & \hat{Q}_{12}^{(1)}\Lambda_{22}^{(1)} & 0 \\ \hat{Q}_{12}^{(1)}\Lambda_{22}^{(1)} & \dfrac{(\hat{Q}_{12}^{(1)})^2}{\hat{Q}_{11}^{(1)}}\Lambda_{22}^{(1)} & 0 \\ 0 & 0 & \hat{Q}_{66}^{(1)}\Lambda_{66}^{(1)} \end{bmatrix} \qquad [R^{(2)}] = \begin{bmatrix} \dfrac{(\hat{Q}_{12}^{(1)})^2}{\hat{Q}_{22}^{(2)}}\Lambda_{22}^{(1)} & \hat{Q}_{12}^{(1)}\Lambda_{22}^{(1)} & 0 \\ \hat{Q}_{12}^{(1)}\Lambda_{22}^{(1)} & \hat{Q}_{22}^{(1)}\Lambda_{22}^{(1)} & 0 \\ 0 & 0 & \hat{Q}_{66}^{(1)}\Lambda_{66}^{(1)} \end{bmatrix} \tag{17}$$

The In-situ Damage Effective Functions $\Lambda_{22}^{(\mu)}, \quad \Lambda_{66}^{(\mu)}$ introduced in [21-23] can be expressed in terms of macrostresses and macrostrains in the μ^{th} layer of the $\text{ECM}\mu$ as

$$\Lambda_{22}^{(1)} = 1 - \frac{\overline{\sigma}_{11}^{(1,1)}}{\hat{Q}_{11}^{(1)}\overline{\varepsilon}_1^{(1,1)} + \hat{Q}_{12}^{(1)}\overline{\varepsilon}_2^{(1,1)}}, \qquad \Lambda_{22}^{(2)} = 1 - \frac{\overline{\sigma}_{22}^{(2,2)}}{\hat{Q}_{12}^{(2)}\overline{\varepsilon}_1^{(2,2)} + \hat{Q}_{22}^{(2)}\overline{\varepsilon}_2^{(2,2)}} \tag{18a}$$

$$\Lambda_{66}^{(\mu)} = 1 - \frac{\overline{\sigma}_{12}^{(\mu,\mu)}}{\hat{Q}_{66}^{(\mu)}\overline{\varepsilon}_6^{(\mu,\mu)}} \tag{18b}$$

On substituting macrostresses, calculated from Eqs. (13), and macrostrains, calculated from Eq. (15), into Eq. (18), the closed form expressions for IDEFs are obtained. They represent $\Lambda_{22}^{(\mu)}, \quad \Lambda_{66}^{(\mu)}$ as functions of relative cracking/splitting

density $D_\mu^{mc} = h_\mu / s_\mu$, relative delamination area $D_\mu^{ld} = \ell_\mu / s_\mu$, the layer compliances $\hat{S}_{ij}^{(\mu)}, S_{ij}^{(\kappa)}, \kappa \neq \mu$, shear lag parameters K_j and the layer thickness ratio χ

$$\Lambda_{qq}^{(\mu)} = \Lambda_{qq}^{(\mu)}(D_\mu^{mc}, D_\mu^{ld}, \hat{S}_{ij}^{(\mu)}, S_{ij}^{(\kappa)}, K_j, \chi) \tag{19}$$

In detail, the closed form expressions for the IDEFs for the μ^{th} layer of the $\text{ECM}\mu$ are

$$\Lambda_{22}^{(\mu)} = 1 - \frac{1 - \dfrac{D_\mu^{mc}}{\lambda_1^{(\mu)}(1-D_\mu^{ld})}\tanh\left[\dfrac{\lambda_1^{(\mu)}(1-D_\mu^{ld})}{D_\mu^{mc}}\right]}{\dfrac{1+\lambda_1^{(\mu)}D_\mu^{ld}}{1-D_\mu^{ld}} + \alpha_1^{(\mu)}\dfrac{D_\mu^{mc}}{\lambda_1^{(\mu)}(1-D_\mu^{ld})}\tanh\left[\dfrac{\lambda_1^{(\mu)}(1-D_\mu^{ld})}{D_\mu^{mc}}\right]}, \quad \mu = 1,2, \tag{20a}$$

$$\Lambda_{66}^{(\mu)} = 1 - \frac{1 - \dfrac{D_\mu^{mc}}{\lambda_2^{(\mu)}(1-D_\mu^{ld})}\tanh\left[\dfrac{\lambda_2^{(\mu)}(1-D_\mu^{ld})}{D_\mu^{mc}}\right]}{\dfrac{1+\lambda_2^{(\mu)}D_\mu^{ld}}{1-D_\mu^{ld}} + \alpha_2^{(\mu)}\dfrac{D_\mu^{mc}}{\lambda_2^{(\mu)}}\tanh\left[\dfrac{\lambda_2^{(\mu)}(1-D_\mu^{ld})}{D_\mu^{mc}}\right]}, \quad \mu = 1,2 \tag{20b}$$

where the constants $\lambda_i^{(\mu)}, \alpha_i^{(\mu)}, i = 1,2$ (Appendix C of [26]) depend solely on the layer compliances $\hat{S}_{ij}^{(\mu)}, S_{ij}^{(\kappa)}, \kappa \neq \mu$, shear lag parameters K_j and the layer thickness ratio χ. The modified compliances $S_{ij}^{(\kappa)}, \kappa \neq \mu$ of the equivalently constraining' κ^{th} layer of the $\text{ECM}\mu$ are determined from the analysis of the $\text{ECM}\kappa$ and therefore are functions of the IDEFs $\Lambda_{22}^{(\kappa)}, \Lambda_{66}^{(\kappa)}$. Thus, the IDEFs for the μ^{th} layer depend implicitly on the damage parameters $D_\kappa^{mc} = h_\kappa / s_\kappa, D_\kappa^{ld} = h_\kappa / \ell_\kappa$ associated with the κ^{th} layer.

The IDEFs for both layers form a system of simultaneous nonlinear algebraic equations

$$\Lambda_{qq}^{(1)} = \Lambda_{qq}^{(1)}(D_1^{mc}, D_1^{ld}, \hat{S}_{ij}^{(1)}, S_{ij}^{(2)}(D_2^{mc}, D_2^{ld}, \hat{S}_{ij}^{(2)}, \Lambda_{qq}^{(2)}), \chi), \quad q = 2,6 \tag{21a}$$

$$\Lambda_{qq}^{(2)} = \Lambda_{qq}^{(2)}(D_2^{mc}, D_2^{ld}, \hat{S}_{ij}^{(2)}, S_{ij}^{(1)}(D_1^{mc}, D_1^{ld}, \hat{S}_{ij}^{(1)}, \Lambda_{qq}^{(1)}), \chi), \quad q = 2,6 \tag{21b}$$

This system is solved computationally using a direct iterative procedure. It is carried out in such a way that the newly calculated IDEFs $\Lambda_{qq}^{(\mu)}$ are used to evaluate the reduced stiffnesses of the equivalently constraining κ^{th} layer repeatedly until the difference between two iterative steps meets the prescribed accuracy. Consequently, all four IDEFs $\Lambda_{qq}^{(k)}, q = 2,6\ k = 1,2$ are determined as functions of damage parameters $D_1^{mc}, D_2^{mc}, D_1^{ld}, D_2^{ld}$. If interactions between damage modes in different laminae are neglected, IDEFs associated with the μ^{th} layer will depend only on damaged parameters for that layer.

Verification of the ECM/2-D shear lag approach in absence of crack-induced delaminations was carried out in [15, 17, 19, 27]. After comparison with other existing models by Hashin [28], Tsai and Daniel [29] and Henaff-Gardin et al [30, 31] describing stiffness reduction of CFRP and GFRP cross-ply laminates due to transverse cracking and splitting, the following conclusions were reached in [15]. As far as the reduction of the Young's modulus is concerned, the ECM/2-D shear la approach is in very good agreement with other models. Its predictions are closer to the lower bound established by Hashin [28] than the results of Henaff-Gardin et al [30,]. For the Poisson's ratio, the ECM/2-D shear lag approach predictions are close to those of Henaff-Gardin et al [30], although for small values of the damage parameter (relative crack/split spacing) the reduction predicted by the ECM/2-D shear lag approach is greater than of Henaff-Gardin et al [30. Predictions based on the variational approach of Hashin [28] are far away from these results. The shear modulus reduction ratio predicted by Tsai and Daniel [29] is, in the most of cases, within 10% of the ECM/2-D shear lag approach value.

It is worth mentioning here that the model of Tsai and Daniel [29] and the present ECM/2-D shear lag approach yield exactly the same analytical expression for the shear modulus reduction ratio due to transverse cracking, if the thickness of the shear layer in the ECM/2-D shear lag approach is taken equal to that of the 0^{o} lamina, i.e. if $h_s = h_1$:

$$\rho_G \equiv \frac{G_A}{\hat{G}_A} = \left[1 + \frac{1}{\chi}\frac{D_2^{mc}}{\lambda_2^{(2,2)}}\tanh\frac{\lambda_2^{(2,2)}}{D_2^{mc}}\right]^{-1} \tag{22}$$

For transverse cracking combined with splitting, Tsai and Daniel [29] suggested a semi-empirical expression for the shear modulus reduction ratio based on the "superposition" of solutions for a single set of cracks as

$$\rho_G = \left[1 + \chi\frac{D_1^{mc}}{\lambda_2^{(1,1)}}\tanh\frac{\lambda_2^{(1,1)}}{D_1^{mc}} + \frac{1}{\chi}\frac{D_2^{mc}}{\lambda_2^{(2,2)}}\tanh\frac{\lambda_2^{(2,2)}}{D_2^{mc}}\right]^{-1} \tag{23}$$

The value of the shear modulus reduction ratio obtained by Tsai and Daniel [29] using the finite difference iteration appeared to be within 1% of the value given by Eq. (23). The present ECM/2-D shear lag model, if the interaction between transverse cracks and splits is neglected and the shear layer has the thickness of the 0^o lamina, yields an expression

$$\rho^*_G = \left[1 - \underline{\underline{\frac{D_1^{mc}}{\lambda_2^{(1,1)}} \frac{D_2^{mc}}{\lambda_2^{(2,2)}} \tanh\frac{\lambda_2^{(1,1)}}{D_1^{mc}} \tanh\frac{\lambda_2^{(2,2)}}{D_2^{mc}}}}\right] \times$$
$$\times \left[1 + \chi \frac{D_1^{mc}}{\lambda_2^{(1,1)}} \tanh\frac{\lambda_2^{(1,1)}}{D_1^{mc}} + \frac{1}{\chi}\frac{D_2^{mc}}{\lambda_2^{(2,2)}} \tanh\frac{\lambda_2^{(2,2)}}{D_2^{mc}} + \underline{\underline{\frac{D_1^{mc}}{\lambda_2^{(1,1)}} \frac{D_2^{mc}}{\lambda_2^{(2,2)}} \tanh\frac{\lambda_2^{(1,1)}}{D_1^{mc}} \tanh\frac{\lambda_2^{(2,2)}}{D_2^{mc}}}}\right]^{-1} \quad (24)$$

It may be seen from Eqs. (23) and (24) that the two expressions differ by the underlined terms and $\rho^*_G \le \rho_G$. In absence of splitting $(D_1^{mc} = 0)$ they are both reduced to Eq. (22). In some cases, though, the error of the semi-empirical expression, Eq. (23) suggested by Tsai and Daniel [29] can be as big as 20%. The ECM/2-D shear lag approach is in good agreement with the results of Henaff-Gardin et al [30] for the shear modulus reduction.

Results and discussion

Stiffness degradation in cross-ply laminates due to different damage modes and their combinations is examined below. All results given below were obtained taking into account the interaction between damage modes in the adjacent layers. Up to 12 iterations are required to solve a set of simultaneous non-linear equations, Eqs. (21) with accuracy of 10^{-9}. The number of iterations increases along with the crack density and relative delamination area.

Figure 4 shows stiffness degradation in E-glass/LY556 epoxy [26] $[0/90/0]$ and $[0/90_8/0]$ cross-ply laminates as the function of the transverse crack density C_2 in the $90°$ layer. The layers thicknesses h_1 and h_2 are determined from the laminate lay-up, thickness of the shear layer is taken as $h_s = t$. Longitudinal Young' modulus, shear modulus and major Poisson's ratio are normalised by their values in the undamaged state. As can be seen from Fig. 4a,b, all these properties undergo degradation as the matrix crack density increases, with Poisson's ratio appearing to be the most affected by transverse cracking. The thickness of the $90°$ layers play an important role, since the thicker the $90°$ layer, the bigger reduction is observed. Transverse ply thickness and the thickness ratio of $90°$ layer to constraining $0°$ layers are the important parameters controlling resistance to matrix cracking. Zhang, Fan and Soutis [23] proposed to use a resistance curve, analogous to the R-curve concept of classical fracture mechanics, as a measure of the composite resistance to crack initiation and growth

$$G(\sigma, D^{mc}) = G_R(D^{mc}), \quad G_R = G_{IC} + G_0(1 - \exp(-RD^{mc})) \quad (25)$$

where G is the strain energy release rate associated with matrix cracking, G_R is the laminate resistance to matrix cracking, G_{IC} is the critical energy release rate for damage nucleation, and G_0 and R are laminate constants. Parameters G_{IC}, G_0 and R are not independent of stacking sequence, but remain constant as long the thickness ratio of the constraining layer to $90°$ remains the same.

When a cross-ply laminate is subjected to biaxial loading matrix cracking may occur concurrently in both plies leading to formation of transverse and longitudinal matrix cracks. The combined effect of these cracks on stiffness properties of $[0/90/0]$ laminate is shown in Fig. 5 for the case when the longitudinal and transverse crack densities are equal.
In cross-ply laminates with thick $90°$ layer subjected to uniaxial loading strip-shaped delaminations begin to initiate and grow from the tips of matrix cracks at the $0°/90°$ interface. The effect of these delaminations on stiffness properties of $[0/90_8/0]$ laminate is shown in Fig. 6 as a function of relative delamination area. Transverse crack density is taken as 2 cracks/cm, and the values of normalised stiffness properties for $D_2 = 0$ correspond to stiffness degradation due to matrix cracking without delamination. It can be seen from Fig. 6 that crack-tip delamination contributes significantly to stiffness degradation of the laminate, and therefore has to be taken into account in the post-initial failure models.

Figure 7 shows stiffness degradation in T800H/3631 carbon/epoxy $[0/90_n]_s$, $n = 2,4,6$ cross-ply laminates containing transverse cracks and delaminations. Longitudinal Young's modulus, in-plane shear modulus and Poisson's ratio, normalised by their values in the undamaged state, are plotted as a function of transverse crack density. The relative delamination area is 10%, which corresponds to $\ell/s = 0.1$. For the axial modulus, predictions are compared to experimental data obtained by Takeda and Ogihara [32] and appear to be in good agreement. However, predictions show that reduction in shear modulus and Poisson's ratio due to crack tip delamination is more significant.

Henaff-Gardin et al [31] observed damage development in cross-ply $[0_4/90_4]_s$ T300/914 carbon/epoxy laminates during thermal cycling. The cycle consisted of cooling to –200°C and heating to +90°C. Crack density in the 90° and 0° plies was measured, however the size of growing delaminations that accompanied longitudinal cracks was not. In Fig. 8a, predictions of reduction in the longitudinal Young's modulus, shear modulus and Poisson's ratio, normalised by their values in the undamaged state, are shown along with the measured crack densities in the 90° and 0° plies as a function of number of cycles. As cracks develop, the shear modulus and Poisson's ratio undergo significant reduction, while reduction in axial modulus remains less than 5%. This indicates that the shear modulus and the Poisson's ratio could be much better parameters to characterise stiffness degradation of the laminate than the longitudinal modulus.

Since the size of the delamination area was not measured during cycling, reduction of stiffness properties of $[0_4/90_4]_s$ T300/914 laminate due to delaminations was predicted using assumed delamination sizes. Strip-width of the transverse delamination was set to zero, while that of the longitudinal delamination allowed to vary from zero to 50%. In other words, longitudinal delaminations were assumed to have propagated from the crack tip to one quarter of the distance between two cracks. This seems to be a reasonable assumption, consistent with X-ray radiographs obtained by Henaff-Gardin et al [31]. In Figs. 8b and 8c, predicted reductions of the longitudinal, transverse and shear moduli as well as Poisson's ratio, normalized by their values in the undamaged state, are plotted as function of the relative delamination area. The axial modulus appears to be unaffected by the growth of delamination, while transverse modulus is further reduced, but not significantly (Fig. 8b). The reduction in the shear modulus is more pronounced than in the Poisson's ratio (Fig. 8c). Crack densities in 90° and 0° plies were taken as C_2=4.5 cracks/cm and C_1=3 cracks/cm respectively, which corresponds to saturation values reached during –200°C/+90°C cycling. Under uniaxial loading, longitudinal delaminations appear to be more important than the transverse ones, since they result in isolation of the portions of the load-bearing 0° plies, which become prone to fibre breakage. Under biaxial loading, the importance of one set of delaminations over the other depends very much on the biaxiality and ply thickness ratios.

Conclusions

Although the approach described in this paper has not attempted to predict ultimate laminate failure, it does present a methodology for predicting degraded stiffness properties of the laminae and hence the laminate, in the case when there are various kinds of intra- and interlaminar damage interacting with each other are present in the same and/or adjacent plies of the laminate. The approach is based on the Equivalent Constraint Model (ECM) of the damaged laminate and takes into account damage mode interaction. Our predictions show that the effect of longitudinal matrix cracking is more pronounced on the Poisson's ratio than on the shear modulus; however the reduction in the shear modulus due to transverse delamination is the most significant when compared to the reduction observed in the axial or transverse elastic moduli.

Theoretically, ECM does not impose any restrictions onto the laminate lay-up, and the approach based on ECM was successfully applied to the prediction of degraded stiffness properties due to matrix cracking in all but $0°$ layers of quasi-isotropic laminates. It should be noted that for the model to be applied the type, location and amount of damage present need to be specified. For this accurate and reliable structural health monitoring (SHM) techniques are urgently required, see Soutis and coworkers [33-35]. Also the triggering of resin cracking and delamination could be delayed to higher applied loads if tougher resin systems are employed, Jumahat et al. [36].

Competing Interests

We have no competing interests

Funding

Financial support of this research by the Engineering and Physical Sciences Research Council (EPSRC/GR/L51348) and the British Ministry of Defence is gratefully acknowledged.

References

1. Kashtalyan M., Soutis C. 2002. Mechanisms of internal damage and their effect on the behavior and properties of cross-ply composite laminates. *International Applied Mechanics* **38**, 641-657.

2. Kashtalyan M., Soutis C. 2005. Analysis of composite laminates with intra- and interlaminar damage. *Progress in Aerospace Sciences* **41**, 152-173.

3. Rebiere J.-L., Gamby D. 2004. A criterion for modelling initiation and propagation of matrix cracking and delamination in cross-ply laminates. *Composites Science and Technology* **64**, 2239-2250.

4. Rebiere J.-L., Gamby D. 2008. A decomposition of the strain energy release rate associated with the initiation of transverse cracking, longitudinal cracking and delamination in cross-ply laminates. *Composite Structures* **84**, 186-197.

5. Lim, S.-H. and Li, S. 2005. Energy reslease rate for transverse cracking and delamination induced by transverse cracks

in laminated composites. *Composites Part A: Applied Science and Manufacturing* **36**, 1467-1476.
6. Blazques A., Mantic V., Paris F. and McCartney L.N. 2008. Stress state characterisation of delamination cracks in [0/90] symmetric laminates by BEM. *International Journal of Solids and Structures* **45**, 1632-1662
7. Maimi P., Camanho P.P., Mayugo J.A. and Turon A. 2011. Matrix cracking and delamination in laminated composites. Part I: Ply constitutive law, first ply failure and onset of delamination. *Mechanics of Materials* **434**, 169-185
8. Maimi P., Camanho P.P., Mayugo J.A. and Turon A. 2011. Matrix cracking and delamination in laminated composites. Part II: Evolution of crack density and delamination. *Mechanics of Materials* **43**, 194-211
9. Garcia I.G., Mantic V., Blazquez A. and Paris F. 2014.Transverse crack onset and growth in cross-ply $[0/90]_s$ laminates under tension. Application of a coupled stress and energy criterion. *International Journal of Solids and Structures* **51**, 3833-3856.
10. Shi Y., Pinna C., Soutis C. 2014. Modelling impact damage in composite laminates: A simulation of intra- and inter-laminar cracking. *Composite Structures* **114**, 10-19.
11. Shi Y., Soutis C. 2016. Modelling transverse matrix cracking and splitting of cross-ply composite laminates under four point bending. *Theoretical and Applied Fracture Mechanics*, in press.
12. Kashtalyan M., Soutis C. 1999. A study of matrix crack tip delaminations and their influence on composite laminate stiffness. *Advanced Composites Letters* **8**, 149-156..
13. Kashtalyan M., Soutis C. 1999. Application of the Equivalent Constraint Model to investigate stiffness properties of transversally cracked and split FRP laminates. *Advanced Composites Letters* **8**, 205-211.
14. Kashtalyan M., Soutis C. 2000. The effect of delaminations induced by transverse cracking and splitting on stiffness properties of composite laminates. *Composites: Part A* **31**, 107-119.
15. Kashtalyan M., Soutis C. 2000. Stiffness degradation in cross-ply laminates damaged by transverse cracking and splitting. *Composites: Part A* **31**, 335-351.
16. Kashtalyan M., Soutis C. 2000. Modelling stiffness degradation due to matrix cracking in angle-ply composite laminates. *Plastics, Rubber and Composites* **29**, 482-488.
17. Kashtalyan M., Soutis C. 2001. Strain energy release rate for off-axis ply cracking in laminated composites. *International Journal of Fracture* **112**, L3-L8.
18. Kashtalyan M., Soutis C. 2002. Analysis of local delaminations in composite laminates with angle ply matrix cracks. *International Journal of Solids and Structures* **39**, 1515-1537.
19. Soutis C., Kashtalyan M. 2002. Delamination growth and residual properties of cracked orthotropic laminates under tensile loading. *Journal of Thermoplastic Composite Materials* **15**, 13-22.
20. Kashtalyan M., Soutis C. 2006. Modelling off-axis ply matrix cracking in continuous fibre-reinforced polymer matrix composite laminates. *Journal of Materials Science* **41**, 6789-6799.
21. Kashtalyan M., Soutis C. 2007. Stiffness and fracture analysis of laminated composites with off-axis ply matrix cracking. *Composites Part A: Applied Science and Manufacturing* **38**, 1262-1269
22. Zhang J., Fan J. and Soutis C. 1992. Analysis of multiple matrix cracking in $[\pm\theta_m/90_n]_s$ composite laminates Part 1: In-plane stiffness properties. *Composites* **23**, 291-298
23. Zhang J., Fan J. and Soutis C. 1992. Analysis of multiple matrix cracking in $[\pm\theta_m/90_n]_s$ composite laminates Part 2: Development of transverse ply cracks. *Composites* **23**, 299-304
24. Fan J., Zhang J. 1993. In-situ damage evolution and micro/macro transition for laminated composites. *Composites Science and Technology* **47**, 107-118.
25. Zhang J. and Herrmann K.P. 1999. Stiffness degradation induced by multilayer matrix cracking in composite laminate. *Composites Part A* **30**, 683-706
26. Kashtalyan M., Soutis C. 2013. Predicting residual stiffness of cracked composite laminates subjected to multi-axial inplane loading. *Journal of Composite Materials* **47**, 2513-2524.
27. Katerelos D.T.G., Kashtalyan M., Soutis C., Galiotis C. 2008. Matrix cracking in polymeric composites laminates. Modelling and experiments. *Composites Science and Technology* **68**, 2310-2317.
28. Hashin Z. 1987. Analysis of orthogonally cracked laminate under tension. *Transactions of ASME Journal of Applied Mechanics* **54**, 872-879.
29. Tsai C.L., Daniel I.M. 1992. Behavior of cracked cross-ply composite laminate under shear loading. *International Journal of Solids and Structures* **29**, 3251-3267.
30.Henaff-Gardin C., Lafarie-Frenot M.C., Gamby D. 1996a. Doubly periodic matrix cracking in composite laminates Part 1: General in-plane loading. *Composite Structures* **36**, 113-130.
31. Henaff-Gardin C., Lafarie-Frenot M.C., Gamby D. 1996b. Doubly periodic matrix cracking in composite laminates Part 2: Thermal biaxial loading. *Composite Structures* **36**, 131-140.
32. Takeda N., Ogihara S. 1994. Initiation and growth of delamination from the tip of transverse cracks in CFRP cross-ply laminates. *Composites Science and Technology* **52**, 309-318
33. Diaz Valdes S.H. and Soutis C. 2000. Health monitoring of composites using Lamb waves generated by piezo-electric devices. *Plastics, Rubber and Composites* **29**, 496-502.
34. Diamanti K., Soutis C. and Hodgkinson J. M. 2005. Lamb waves for the non-destructive inspection of monolithic and sandwich composite beams. *Composites A* **36**, 189-195.
35. Diamanti K. and Soutis C. 2010. Structural health monitoring techniques for aircraft composite structures. *Progress in Aerospace Sciences* **46**, 343-352.
36. Jumahat A., Soutis C., Jones F.R. and Hodzic A. 2010. Fracture mechanisms and failure analysis of carbon fibre/toughened epoxy composites subjected to compressive loading. *Composite Structures* **92**, 295-305.

For Peer Review Only

Figures

Figure 1. Cross-ply laminate damaged by transverse and longitudinal matrix cracks and transverse and longitudinal crack-induced delaminations.

Figure 2. Equivalent Constraint Model (ECM) of a damaged laminate: a) initial laminate; b) ECM*k*.

Figure 3. Representative segments of the two equivalent constraint models: a) ECM1; b) ECM2.

Figure 4. Normalised stiffness properties of E-glass/LY556 epoxy cross-ply laminates as a function of transverse crack density in the $90°$ layer: a) $[0/90/0]$ laminate; b) $[0/90_8/0]$ laminate. No damage in the $0°$ layer (uniaxial tensile loading, static or fatigue).

Figure 5. Normalised stiffness properties of E-glass/LY556 epoxy $[0/90/0]$ cross-ply laminate as a function of transverse crack density in the $90°$ layer, equal to longitudinal crack density (equi-biaxial tensile static or fatigue loading).

Figure 6. Normalised stiffness properties of E-glass/LY556 $[0/90_8/0]$ cross-ply laminate as a function of transverse delamination area. Transverse crack density 2 cracks/cm (uniaxial tensile loading).

Figure 7. Stiffness reduction due to transverse crack tip delaminations in T800H/3631 carbon/epoxy cross-ply laminates as a function of crack density: a) $[0/90_2]_s$; b) $[0/90_4]_s$; c) $[0/90_6]_s$.

Figure 8. Stiffness reduction in a $[0_4/90_4]_s$ T300/914 carbon/epoxy laminate subjected to –200°C/+90°C thermal cycling: a) stiffness reduction due to matrix cracking and matrix crack density as a function of number of cycles; b) longitudinal and transverse moduli reduction due to longitudinal crack tip delamination as a function of delamination area D^{ld}; c) shear modulus and Poisson's ratio reduction due to longitudinal crack tip delamination as a function of delamination area D^{ld}.

For Review Only

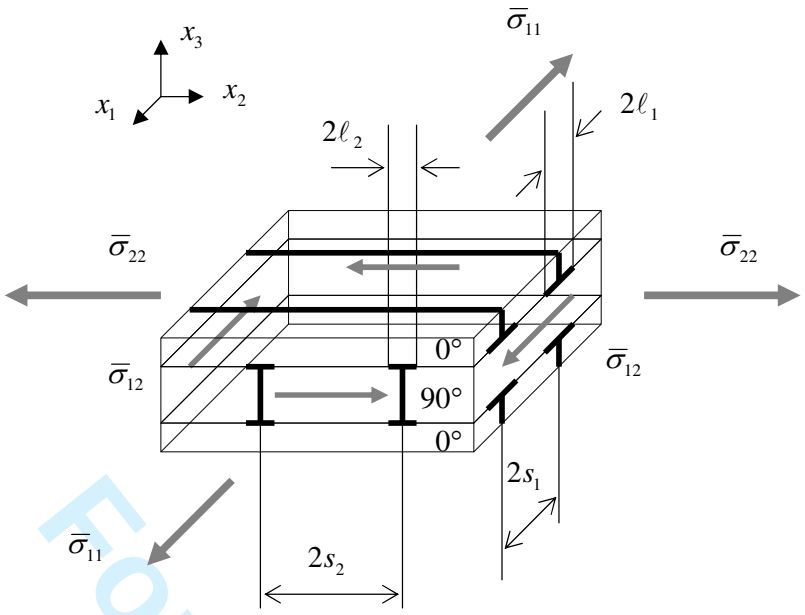

Figure 1

For Review Only

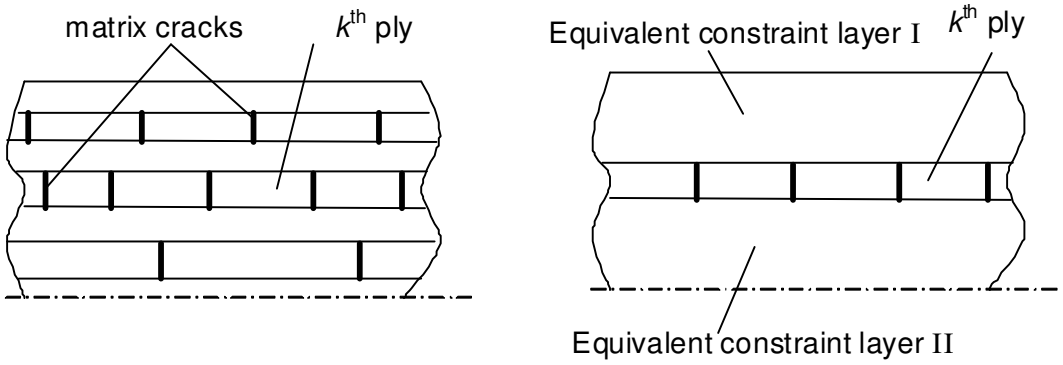

Figure 2

For Review Only

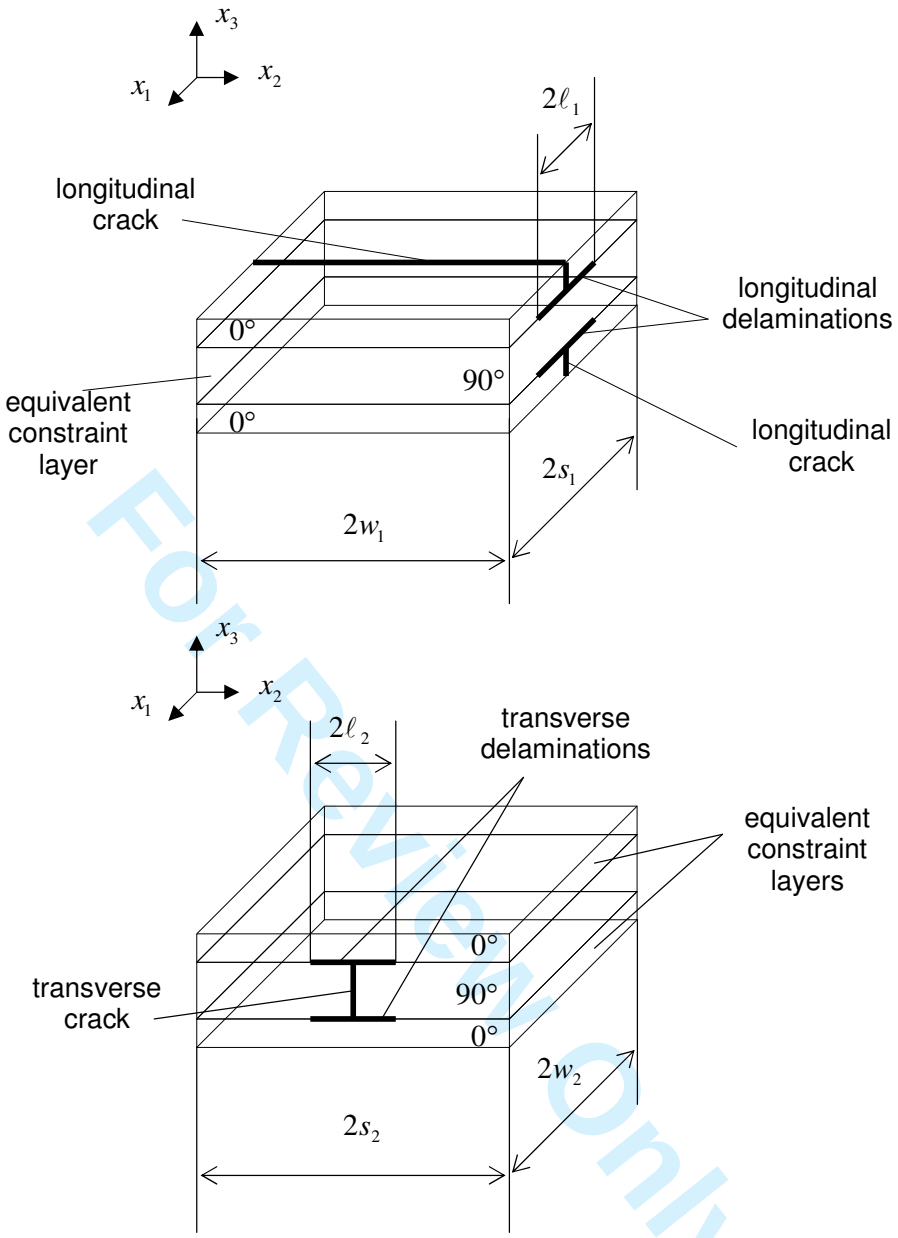

Figure 3

For Review Only

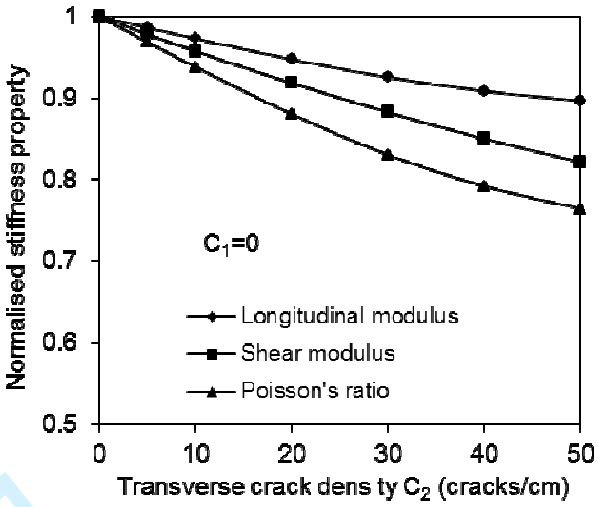

a)

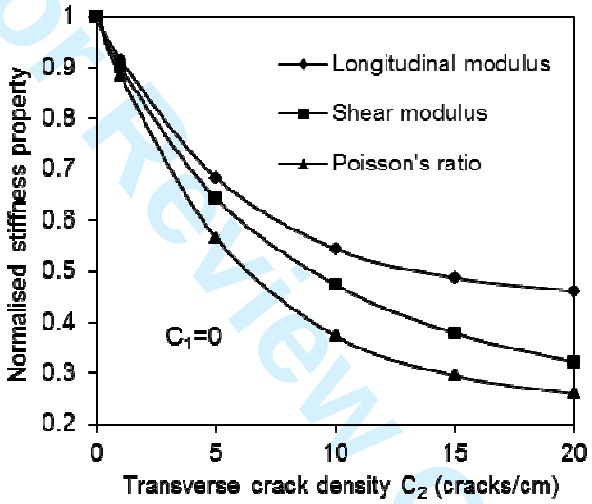

b)

Figure 4

For Review Only

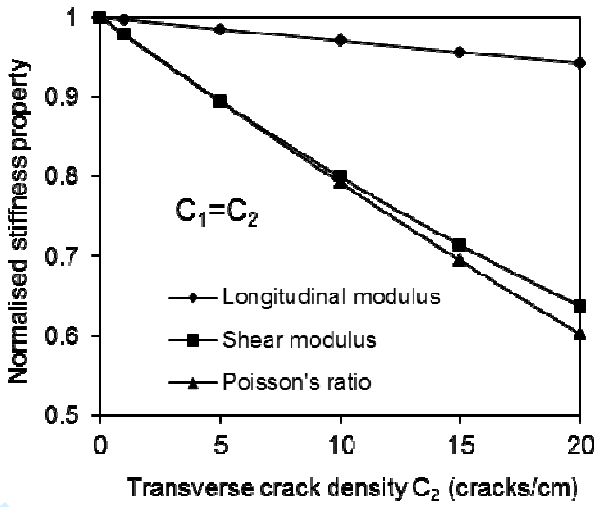

Figure 5

For Review Only

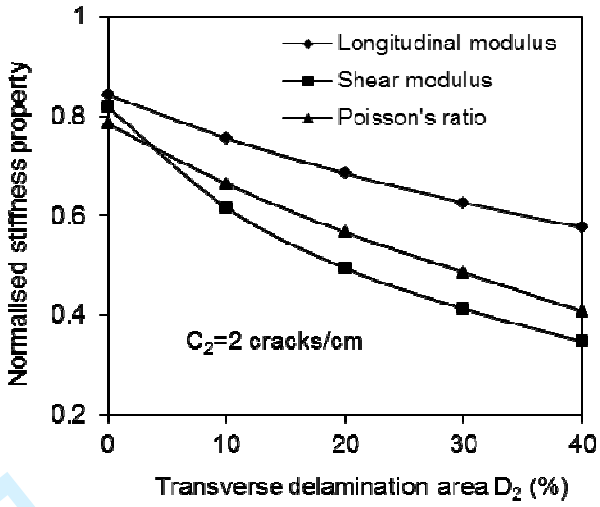

Figure 6

For Review Only

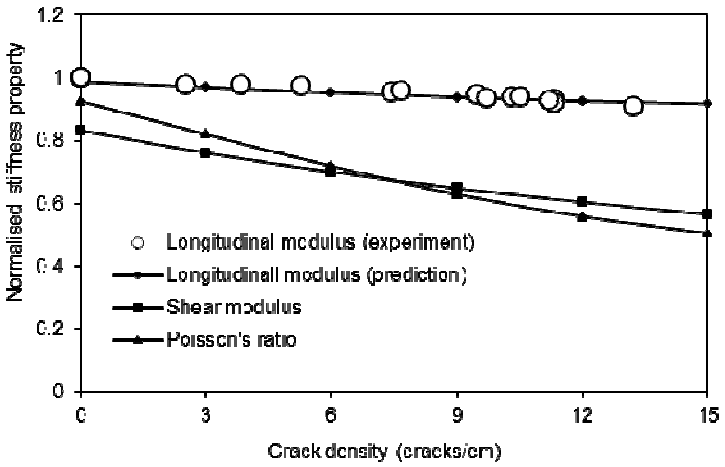

a)

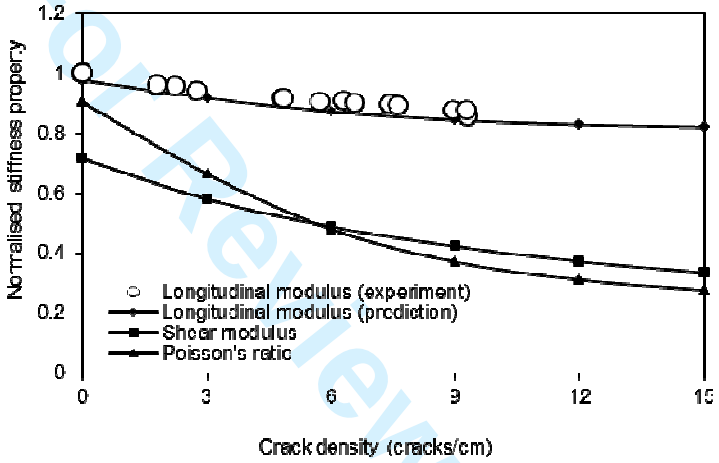

b)

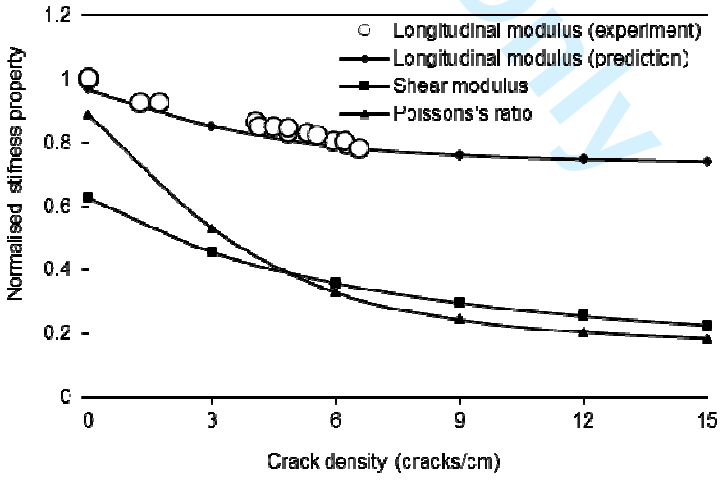

c)

Figure 7

For Review Only

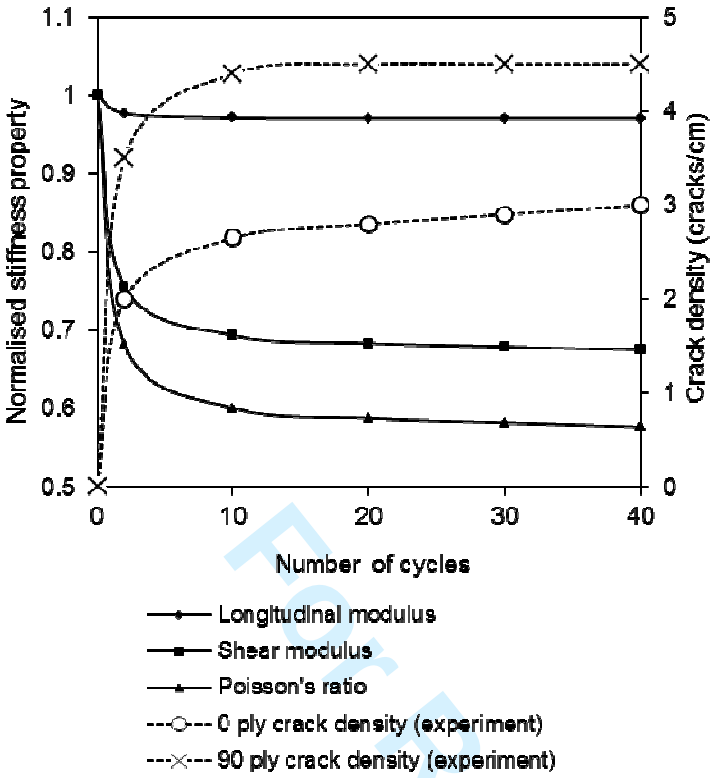

a)

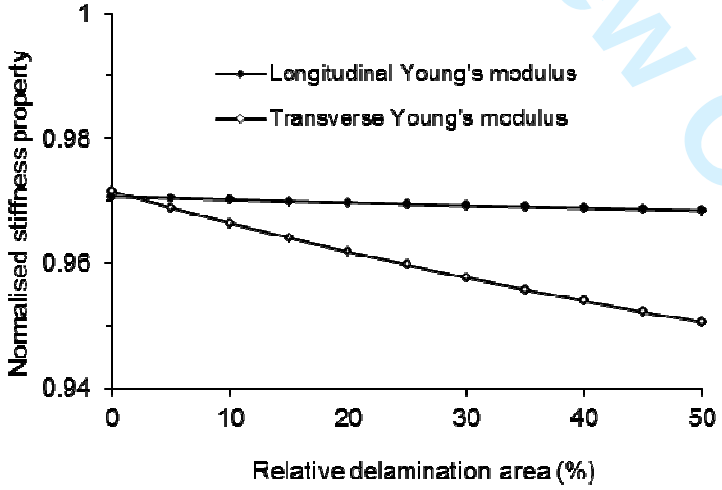

b)

For Review Only

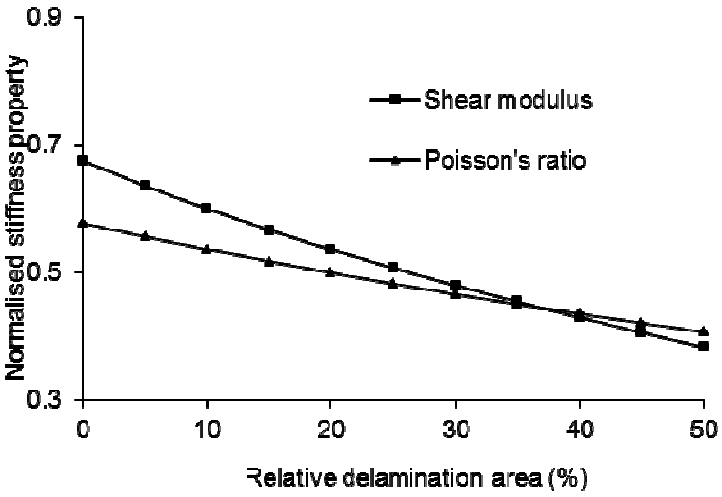

c)

Figure 8.

For Review Only